Green's function estimation using secondary sources in a shallow water environment

Philippe Roux, Mathias Fink

Green's function estimation using secondary sources in a shallow water environment

Article *in* The Journal of the Acoustical Society of America · April 2003

DOI: 10.1121/1.1542645 · Source: PubMed

2 authors:

Philippe Roux
University Grenoble Alpes
494 PUBLICATIONS **12,931** CITATIONS
SEE PROFILE

Mathias Fink
École Supérieure de Physique et de Chimie Industrielles
1,029 PUBLICATIONS **55,461** CITATIONS
SEE PROFILE

Green's function estimation using secondary sources in a shallow water environment

Philippe Roux [1,2] and Mathias Fink,

Laboratoire Ondes et Acoustique, ESPCI, Université Paris VII,

10 rue Vauquelin, 75005 Paris, France.

PACS numbers: 43.30.k, 43.60.Gk

[1] Corresponding author.
[2] Currently at the Marine Physical Laboratory, Scripps Institution of Oceanography, UCSD, San Diego.

Abstract

This work deals with a new way to measure the Green's function between two points in an acoustic channel without emitting a pulse by any of the two points. The Green's function between A and B is obtained from a set of secondary sources in the guide by averaging either the correlation or the convolution of the signals received in A and B. A theoretical approach based on mode propagation in a monochromatic regime is presented. Results are then extended to the time-domain. Estimation of the Green's function is performed numerically in a range-independent and a range-dependent environment. Application to discreet acoustic communications is discussed.

Introduction

In a shallow water environment, acoustic communication is limited by reverberation and multipath propagation that generate multiple echoes interfering with each other. In general, the presence of multiple echoes blurs the information to be transmitted. One way to overcome this difficulty is to work with an array of transducers and to use the impulse response (or Green's function) between every element of the array and the receiver. Experimentally, this is naturally done during a time-reversal experiment : a first stage consists in recording the impulse response between every transducer of a time-reversal mirror (TRM) and the desired focal point. In a second stage, the time-reversal version of the Green's functions acts as a natural filter for acoustic communication without any distortion due to waveguide interfaces. Several authors have studied the efficiency and the robustness of time-reversal focusing [1-4] and its applications to acoustic communication in underwater acoustics [5, 6]. The advantage of time-reversal is that it requires no a priori knowledge of the propagation medium. Actually, this means that the first stage in the time-reversal process is a learning stage during which the spatio-temporal filter between the sources and the receiver is acquired. However, the recording of the impulse response between the time-reversal mirror and the focal point may be a difficult or even an undesirable step in the case of discrete acoustic communication.

In this paper, we present a way to get the Green's function between two points in a waveguide without emitting a pulse by any of the two points. The Green's function between A and B is obtained from a set of secondary sources S in the guide by averaging either the correlation or the convolution of the signals received in A and B depending on the relative positions of A and B regarding to S. Because no field is sent by A or B, this technique would lead to applications in discrete acoustic communication for which detection of sources are to

be avoided. Furthermore, this method does not require any knowledge of the waveguide characteristics and can be applied in a range-dependent environment.

The paper is structured as followed: in the first part, a theoretical approach shows a way to get the Green's function between two points using a set of secondary sources in the waveguide. Theory is presented in the monochromatic regime and is then extended to the time domain. In section II, numerical results are presented in two configurations: a range dependent and a range independent oceanic waveguide. The accuracy of the estimated Green's function is discussed in terms of time-reversal focusing and a quantitative comparison with the exact Green's function of the waveguide is performed. In the last section, we describe the practical limitations of this technique in an oceanic environment and we discuss possible applications to discrete acoustic communications in shallow water.

Theoretical approach

Figure 1 is a schematic of the waveguide from which the theoretical approach is performed. The question we try to answer is: how does one get the Green's function between points A and B without using A or B as a source? The sources are a set of vertical sources S located between A and B (Fig. 1a) or outside the channel delimited by the points A and B (Fig. 1b). In the two configurations, the sources S cover the whole water column. Practically speaking, S could be a unique source sent from a ship or a plane and that slowly drops from the surface to the ocean bottom emitting regularly an acoustic beacon during its descent. A similar approach has been introduced by several authors working on source localization in shallow water environments using a virtual receiver [7, 8]. The main idea of these works is to use a reference field to correct for oceanic variability. For source localization, use of a reference source can reduce environmental mismatch problem and effectively localize targets [9, 10]. Applied to the configuration described in Fig. 1, it means for example use the field

emitted from A and recorded on the receivers S in order to localize B. In this paper, we proceed in a reciprocal way: by using an ensemble of secondary sources S, we intend to estimate the Green's function between A and B in the time domain.

For a matter of simplicity, the theoretical approach is described in a monochromatic regime. An acoustic beacon sent from S is received by A and B. In a wave guide, the Green's functions between a source in S and receivers in A and B at a frequency ω are written as follows

$$G(S,A) \propto \sum_n U_n(A) U_n(S) \frac{\exp(ik_n R_{SA}) \exp(-\alpha_n R_{SA})}{\sqrt{k_n R_{SA}}} \qquad (1)$$

$$\text{and } G(S,B) \propto \sum_n U_n(S) U_n(B) \frac{\exp(ik_n R_{SB}) \exp(-\alpha_n R_{SB})}{\sqrt{k_n R_{SB}}}, \qquad (2)$$

where n is the mode number, $U_n(x)$ is the amplitude of mode n at depth x, k_n and α_n are the propagating and the attenuation wavenumbers associated to mode n respectively and R_{xy} is the range between x and y. We suppose that the distance R_{AB} is large enough to neglect the contribution to the Green's function G(A,B) of the modal continuum in the penetrable bottom. We make also the approximation that the medium is reciprocal, meaning that fluctuations of the signal due to currents or internal waves are negligible.

Configuration 1: the sources S are located between A and B

Multiplying the Green's functions G(A,S) and G(S,B), we get

$$G(A,S)G(S,B) \propto \sum_m \sum_n U_m(A) U_m(S) U_n(S) U_n(B) \frac{\exp(ik_m R_{AS}) \exp(-\alpha_m R_{AS})}{\sqrt{k_m R_{AS}}} \frac{\exp(ik_n R_{SB}) \exp(-\alpha_n R_{SB})}{\sqrt{k_n R_{SB}}} \qquad (3)$$

.

We suppose now that the sources S are distributed over the whole water column, which allows us to use the orthogonality relation

$$\sum_S U_n(S) U_m(S) \propto \delta_{nm}. \qquad (4)$$

In applying orthogonality it has been assumed that the sources S span the region where the modes have significant amplitude. In addition density gradients have been neglected. Numerical results to be presented later show that these idealizations have little effect on performance, as long as the sources S cover the water column.

Using Eqs. 3 and 4, it follows

$$\sum_S G(A,S)G(S,B) \propto \sum_n U_n(A)U_n(B)\frac{\exp(ik_n R_{AB})\exp(-\alpha_n R_{AB})}{k_n\sqrt{R_{SB}R_{AS}}}, \qquad (5)$$

using the relation $R_{AS}+R_{SB}=R_{AB}$.

In Eq. 5, we recognize the amplitude of the modes in A and B as well as the phase term that describes propagation between A and B. This leads to the conclusion

$$\sum_S G(A,S)G(S,B) \approx G(A,B) \propto \sum_n U_n(A)U_n(B)\frac{\exp(ik_n R_{AB})\exp(-\alpha_n R_{AB})}{\sqrt{k_n R_{AB}}}. \qquad (6)$$

We note obviously that the spreading factor between Eqs. 5 and 6 are not the same but it is a constant factor that has no importance in the estimation of the Green's function. Actually, the difference between Eq. 5 and the true Green's function G(A,B) appears in the amplitude term for each mode in which k_n should be replaced by $\sqrt{k_n}$. Despite this difference, we will see with numerical examples that $\sum_S G(A,S)G(S,B)$ is a good approximation for G(A,B).

Configuration 2 : the sources S are located outside the channel delimited by A and B

In this case, we multiply the Green's function G(A,S) by the phase-conjugated Green's function G(S,B)*,

$$G(A,S)G(S,B)^* \propto \sum_m\sum_n U_m(A)U_m(S)U_n(S)U_n(B)\frac{\exp(ik_m R_{AS})\exp(-\alpha_m R_{AS})}{\sqrt{k_m R_{AS}}}\frac{\exp(-ik_n R_{SB})\exp(-\alpha_n R_{SB})}{\sqrt{k_n R_{SB}}} \qquad (7)$$

Using Eq. 4 and the relation $R_{AS}+R_{SB}=R_{AB,}$ we obtain now

$$\sum_S G(A,S)G(S,B)^* \propto \sum_n U_n(A)U_n(B)\frac{\exp(ik_n R_{AB})\exp(-\alpha_n R_{AB})}{k_n\sqrt{R_{SB}R_{AS}}}\exp(-2\alpha_n R_{SB}) \approx G(A,B)$$

(8)

As in Eq. 5, we recognize in Eq. 8 the modes amplitude and the phase term of the Green's function between A and B. Compared to G(A,B), we once again note the difference in the spreading factor and the amplitude dependence in $1/k_n$. But the main difference lies now in the amplitude modulation of each mode by an exponential decrease that depends on the mode number through the attenuation wavenumber α_n. If $\exp(-2\alpha_n R_{SB})$ is roughly constant from mode to mode, this modulation plays no role in the estimation of the Green's function G(A,B) as the spreading factor $1/\sqrt{R_{SB}R_{AS}}$. However, this is generally not the case and α_n classically increases as a function of the mode number. The contribution of the higher-order modes to the estimated Green's function in this configuration will then be less accurate.

Time-domain solutions

In the first configuration, the result obtained in Eq. 6 can be written in the time-domain as follows

$$G(A,B,t) \approx \sum_S G(A,S,t) * G(S,B,t), \qquad (9)$$

where $*$ refers to convolution. Equation 9 has a well-known physical interpretation : it is the application of Huyghen's theorem. The Green's function between A and B can be seen as the sum over a set of points S, that cover a section of the guide, of the Green's function between A and S convolved with the Green's function between S and B.

In practice though, the sources are in S and receivers are in A and B. Invoking reciprocity, we have $G(A,S,t) = G(S,A,t)$. This leads to another formulation equivalent to Eq. 9

$$G(A,B,t) \approx \sum_S G(S,A,t) * G(S,B,t) \qquad (10)$$

In the second configuration and with the help of reciprocity, the result obtained in Eq. 8 can be written in the time-domain as follows

$$G(A,B,t) \approx \sum_S G(S,A,t) \otimes G(S,B,t), \qquad (11)$$

where $\otimes$ refers now to correlation.

Eqs. 10 and 11 mean that the Green's function between two receivers in a shallow water waveguide can be estimated from a set of secondary sources by either the correlation or convolution of the signals received in A and B.

Eq. 11 has been recently introduced in a remarkable paper [11] by Weaver et al. They experimentally demonstrated for elastic waves in an aluminium sample that the Green's function between points A and B is obtained from a set of secondary sources S by averaging the correlation of the field respectively measured in A and B. What is fascinating in Weaver's approach is that the secondary sources are either acoustic noise from thermal fluctuations inside the sample or deterministic signals from a piezoelectric transducer outside the sample. In underwater acoustics as well as in ultrasonics, this theorem holds only if Eq. 4 is valid. This means, using the language of Weaver that the total energy sent from the secondary sources S is equidistributed over all the modes that are present in the medium. In other words, every mode must be equally excited after summing over the sources S. We wish also to make a strong connection between this work and a paper from Draeger et al [12] on time-reversal in chaotic cavities.

We will see in the following that the Green's function G(A,B,t) can be obtained if the sources S fulfill the following conditions :

- the sources S span the whole water column,
- the depth between two neighboring sources S is such that the highest-order mode that significantly contributes to the Green's function G(A,B) is correctly sampled. The weight of each mode is related to the exponential dependence of the mode amplitude versus range $\exp(-\alpha_n R_{AB})$ as shown in Eq. 6. The attenuation wavenumber α_n depends mostly on the attenuation parameter in the bottom.

However, we will show that an estimation of the Green's function between A and B is still possible even if the secondary sources S do not satisfy these conditions.

Numerical results

The results presented in this paper are obtained with a time-domain simulation performed with a Parabolic Equation code derived from Michael Collins's RAM code [13]. The emitted signal is a gaussian-modulated pulse centered at 200 Hz and whose spectrum ranges from 100 to 300 Hz. The field is synthesized from 200 frequencies, which allow for enough zero-padding to avoid aliasing problems and at the same time allow for a sufficient number of energy-carrying frequencies to resolve time-domain effects. For the computation, five Padé terms are used. The range step is the smallest wavelength λ_{min} = 5 m sent from the source and the depth step is $\lambda_{min}/5$= 1 m.

Two shallow water environments are studied: a range independent and a range dependent waveguide (Fig. 2). The goal of this work is to determine the time-domain impulse response between points A and B from a set of sources S that are located between or outside the two points. One approach to quantify the quality of the estimated Green's function is then to perform a time-reversal experiment between A and B.

Practically speaking, the first step of our work is to obtain the estimated Green's function $\tilde{\tilde{G}}(A_i, B, t)$ between a receiver in B and a set of 25 receivers A_i using a set of sources S_j and Eqs. 10 or 11 (configuration 1 or 2). In order to compare the estimated Green's function $\tilde{\tilde{G}}(A_i, B, t)$ to the true Green's function $G(A_i, B, t)$, we subsequently perform a numerical time-reversal experiment between the time reversal mirror made of the A_i's and B. Thus we also consider B and the A_i's as potential sources in order to compare the accuracy of the algorithm that leads to the estimated Green's functions. Time-reversal will be performed either with the exact Green's functions or the estimated Green's functions. In the introduction,

we described time-reversal as a two-stage process decomposed into a learning process during which the field issued from the source is acquired on the time-reversal mirror, and a back propagation stage that consists of the transmission of the time-reversed field. Here, the comparison is performed by respectively using $\tilde{G}(A_i, B, t)$ or $G(A_i, B, t)$ in the learning stage. It is justified to use time-reversal to quantify the accuracy of the estimated Green's functions because it naturally works as a time-domain correlator or, in other words, as a coherent Bartlett beamformer in the time-domain. As a consequence, time-reversal performed with the estimated Green's functions leads to an ambiguity surface in time and space in which mismatch (leading to high side lobes) are due to an incorrect estimation of the Green's function. A more pedagogical argument in favor of time-reversal is the following: in the frequency domain, the Green's function is a complex number with an amplitude and a phase. To estimate the Green's functions means to get both amplitude and phase right. However they do not have the same relative importance as far as detection, localization or acoustic transmission is concerned. Thus, an estimated Green's function with an exact phase and a wrong amplitude is definitely worthful whereas the contrary is most of the time useless. A classical least-square difference between the estimated and the exact Green's function is interesting (see Figs. 10 and 11) but do not emphasize the respective role played by phase and amplitude in the error. On the contrary, phase conjugation in the frequency domain or time-reversal with time-dependent signals are a good alternative: if the time-reversed field is focused at the original source, this means that, for each frequency, the phase of the estimated Green's function is exact. Furthermore the side lobes amplitude around the source after time-reversal is related to the estimation of the amplitude of the Green's function.

Performing time-reversal to check the accuracy of the estimated Green's function means that we compute in the time domain

$$\mathrm{Refoc}(y,t) = \sum_{A_i} G(B, A_i, -t) * G(A_i, y, t) \qquad (12)$$

$$\text{and } \overline{\text{Refoc}}(y,t) = \sum_{A_i} \tilde{G}(B, A_i, -t) * G(A_i, y, t), \qquad (13)$$

where y refers to depth near point B. Roughly speaking, Refoc (y, t) is the reference time-reversed field around the focal point obtained with the exact Green's functions. This reference time-reversal is now compared to $\overline{\text{Refoc}}(y,t)$ which is computed from the estimated Green's functions.

Range-independent acoustic channel

Figure 3 is a spatial-temporal representation of the exact Green's functions between B and the A_i's after propagation through the channel. As expected, the pressure field is very extended in time due to multiple reflections on the guide interfaces. After propagation through the guide, the field duration is on the order of 0.45 s compared to the 0.02-s duration of the emitted signal. Figure 4 is a spatial temporal representation of the focused field obtained at B after time-reversal from the A_i's. As expected in a classical time-reversal experiment, the field is strongly recompressed in time and space at the initial source. Fig.4 is defined as the reference time-reversal because it has been computed with the exact Green's functions.

In the following, we first work in configuration1, i.e. with the secondary sources S placed between A and B (Fig. 2a). In Fig. 5, we present time-reversed fields obtained with the estimated Green's functions. Two points are important. First, the field is still focused in B and the size of the focal spot remains the same whatever the number of secondary sources S used to estimate the Green's functions. This means that a part of the Green's functions has been estimated correctly which includes a number of modes sufficient to get a narrow focal spot in B. Second, we observe that the side lobe level is strongly dependent on the number of sources S used to compute the estimated Green's functions. It appears that spatial and temporal side lobes remain low as long as the depth step between the sources S is equal or smaller than the

smallest wavelength of the source spectrum λ_{min} = 5 m. We see in Fig.6 that it is not necessary to sample the water column with too many sources S. The time-reversed field in B presents equivalent temporal side lobes with sources S distributed with a 2-m depth step or with a λ_{min}= 5-m. depth step. The estimated Green's functions are close to the exact Green's functions in the two cases. The depth step between two neighboring sources S has to be small enough to provide a correct sampling of the highest-order mode that contributes significantly to the Green's function G(A,B). This depends of course on the frequency, on the absorption in the bottom and on the range between A and B.

On the other hand, the focal spot is clearly distorted if the sources S do not span the entire water column as shown in Fig. 7. In this case, the Green's functions have not been estimated correctly. We observe that side lobes are weaker when the sources S are placed near the bottom than near the surface. This is due to the down-refracting profile of the sound speed that has been used for the computation of the pressure field. In a down-refracting profile, refraction bends acoustic rays toward the ocean bottom. As a consequence, the pressure field is better sampled with an array placed near the bottom than near the surface of the ocean.

According to our theoretical approach, one must satisfy Eq. 4 in order to achieve a good estimation of the Green's functions between the Ai's and B

$$\sum_S U_n(S)U_m(S) \propto \delta_{nm}. \qquad (4)$$

This equation depends only on the number and position of the sources S in the water column. Eq. 4 means that, on average, every mode is similarly excited by the sources S in the ocean channel. The average is performed here by the sum over the sources S in Eqs. 10 and 11. A way to confirm this is to check the validity of Eq. 4 in the four configurations presented in Fig. 5. The sources S span the whole water column and the inter-source distance is varying from 2 m to 20 m. In Fig. 8, we represent the matrix $C_{nm}(S) = \sum_S U_n(S)U_m(S)$ [3], for n and

m varying from 1 to the total number of modes in the waveguide. The modes U_n have been computed at the central frequency of the source (200 Hz) in the acoustic channel described in Fig. 2a. We observe that the matrix $C_{nm}(S)$ is close to the Identity matrix when the spacing between two sources S is equal or less than the acoustic wavelength. On the other hand, a large depth step between neighboring S sources leads to high off-diagonal elements in the matrix $C_{nm}(S)$ (Figs. 8c and 8d) leading to a poor estimation of the estimated Green's functions as shown in Figs. 5c and 8d.

In the following, we try to quantify results shown in Figs. 5 and 8. To this goal we first measure the difference in terms of least square distance between the matrix $C_{nm}(S)$ and the Identity matrix for a large set of sources-S that always span the sources S span the whole water column. Figure 9 shows the standard deviation between $C_{nm}(S)$ and matrix Identity for a number of sources S varying from 1 to 100. We observe that the standard deviation reaches a floor when the number of sources S is such that the depth step between two sources is on the order of the acoustic wavelength. The floor is non-zero because a portion of the energy of each mode is trapped in the sea-bed which is not sampled by the sources S. This means that Eq. 4 is only approximated when modes penetration in the bottom can't be neglected.

In Fig. 10, we compare the exact and the estimated Green's functions in the waveguide in the two configurations shown in Fig. 2a: the sources S are either between points A and B or outside the channel delimited by these two points. When the sources S are between A and B, the Green's function is estimated using Eq. 10 whereas Eq. 11 is used in the other case. For a set of 20 sources S with a 5-m depth step, the two estimated Green's functions are very similar to the exact Green's function. We then extend this comparison by measuring the difference between the exact and the two estimated Green's functions with respect to the number and depths of the sources S. The depths of the sources S are the same as in Fig. 9. We present in Fig. 11 the average standard deviation Std(S) between $\tilde{G}(A_i, B, t)$ and $G(A_i, B, t)$

$$\mathrm{Std(S)} = \sqrt{\frac{\frac{1}{25}\sum_{A_i}\sum_{t}\left(\tilde{G}(A_i,B,t)-G(A_i,B,t)\right)^2}{\frac{1}{25}\sum_{A_i}\sum_{t}G(A_i,B,t)^2}}\,. \qquad (11)$$

Three points are important. First, the results shown in Figs. 9 and 11 are strongly correlated. As expected, the estimated Green's function of Eq. 10-11 are valid if Eq. 4 is satisfied, which provides the respective weight of each mode. In other words, it is possible to get an estimation of the Green's function between two receivers from a set of sources in a waveguide under the condition that every mode is similarly excited by the set of sources. Secondly, in the two configurations shown in Fig. 2a, the standard deviation Std (S) reaches a non-zero floor when the number of sources exceeds a certain number (e.g. N=20). This means that the estimation of the Green's function is not perfect as noted previously when comparing Eqs. 5-8. The amplitude term of the estimated Green's function is at least incorrect by a factor of $\sqrt{k_n}$ for each mode and by an adding factor of $\exp(-2\alpha_n R_{SB})$ in configuration 2. However, the phase term of Eqs. 5 and 8 is correct, which means that the estimated Green's function is accurate enough to focus a field using a time-reversal procedure. Indeed, several ultrasonic works have already shown that the amplitude-dependence of the field has much less importance than the phase dependence of the field as far as phase conjugation or time-reversal is concerned [14]. Last, we see that the floor reached for the standard deviation in Fig. 11 is slightly higher in configuration 2, where the sources S are outside A and B than in configuration 1 where the sources S are between A and B. We show here the influence of the amplitude weight $\exp(-2\alpha_n R_{SB})$ that appears for each mode in Eq. 8. The higher modes estimated using Eq. 8 face an extra attenuation that leads to a small extra error in the amplitude of the time-domain Green's function. This error would significantly increase for larger distances between S and B, i.e. when the sources S are far away from points A and B.

Range-dependent acoustic channel

In the following, we present numerical results obtained in a range dependent acoustic channel. In a slowly-varying range dependent waveguide, Eqs. 1-8 can be rewritten using adiabatic mode theory. In this case, the mode shape depends now on the range and each wavenumber is to be replaced by an average wavenumber over the propagation range. In this work, we deliberately choose the environment described in Fig. 2b, which prevents us to apply modes theory or even adiabatic modes theory between A and B. Therefore, Eqs. 1-8 do not apply and the Green's function can not be described using a simple analytic formulation. However, we numerically show that Eqs. 10-11 still hold, which means that the Green's functions between B and the A_i's can be estimated from a set of secondary sources S that cover the whole water column.

In Figs. 12 and 13, we present results similar to the results of the range-independent waveguide (Figs. 4 and 5). We first compute a classical time-reversal experiment between B and the A_i's using the exact Green's functions in the time-domain. The time-reversed focused field Refoc (y, t) presented in Fig. 12 is once again defined as the reference field. It is interesting to observe that the time-reversed field in B does not present the same pattern as the one obtained in a range-independent waveguide (see Fig. 4). The side lobe level is higher and the size of the focal spot is twice larger. Actually the higher modes present in A and B do no longer exist at the middle of the Chinese-hat shape waveguide and their contribution to the time-reversed focusing have been lost in the sea-bed.

In Fig. 13, we present time-reversed fields obtained with the estimated Green's functions computed from different set of sources S following Eq. 10 (configuration 1). By comparing Refoc (y, t) and $\overline{\text{Refoc}}(y,t)$, we draw the same conclusions as in the case of the range-independent waveguide. Even if we still re-focus in B, the estimated Green's functions are close to the exact Green's functions as long as the depth step between two sources S enables a

good sampling of the higher-order contributing modes. Of course, the range dependency of the channel prevents correlating the accuracy of the estimated Green's functions to either the modal structure of the waveguide or to the way modes are spatially sampled by the set of sources S.

In Fig. 14, we compare the exact and the estimated Green's functions in the two configurations shown in Fig. 2b. When the sources S are between A and B, the Green's function is estimated using Eq. 10 whereas Eq. 11 is used in the other case. Keeping the depth sampling constant (5-m step between two neighboring sources S), the number of sources S is not the same in configuration 1 and 2. As in the range-independent case, the estimated and the exact Green's functions present the same temporal dependence.

We more quantitatively compare the estimated Green's functions to the exact Green's functions by measuring Std(S) in the range-dependent channel. In Fig. 15, we show that results are similar for both the range-dependent and the range-independent waveguides. Two points are important. First, the difference between the estimated Green's functions provided by configuration 1 or 2 relies on the extra attenuation that faces every mode $\exp(-2\alpha_n R_{SB})$ in configuration 2. This error keeps small as long as the sources S are not to far away from points A and B. Secondly, the results obtained with configuration 2 in the range-dependent case shows that Std(S) reaches a floor for 15 sources S whereas 20 sources S are necessary in the range-independent case (see Fig. 11). This is due to the fact that the higher-order modes are lost in the Chinese-hat shape bottom present in the range-dependent environment, thus authorizing a less accurate sampling of the water column by the sources S.

Discussion

In this work, time-domain numerical simulations using a PE code have been performed in the absence of noise. One may wonder if noise in the ocean could degrade the

estimation of the Green's function. The answer is no. Actually, the estimated Green's functions $\tilde{G}(A,B,t)$ are obtained from Eq. 10-11 which imply both either a convolution or a correlation between two fields G(S,A,t) and G(S,B,t) and an average over the set of sources S. The correlation, the convolution and the average are very robust process with respect to random noise. As a consequence, G(S,A,t) and G(S,B,t) may be much more affected by the presence of noise than the estimated Green's function between A and B.

Of course, the main limitation of this method relies on the location of the secondary sources S. We have shown that a good estimation of the Green's function is provided when the sources S are distributed along the whole water column. Even in this case, problems arise when the points A and B are no longer in the same plane as the sources S. Indeed, up to now, we have worked in a 2-D range-dependent or range-independent waveguide. In this case, sources and receivers belong to the same plane, which implies for example $R_{AS}+R_{SB}=R_{AB}$ for sources S placed between the receivers A and B. However, the ocean is of course a 3-D environment and the above relation does not hold when the sources S and the receivers A and B do not belong to the same plane. This is a very important condition because the distance $R_{AS}+R_{SB}$ determines the phase of the estimated Green's function as shown in Eqs. 5-8. An incorrect estimation of the phase leads to an incorrect estimation of the temporal dependence of the Green's function in the time domain, which means no Green's function at all.

An important concern is the nature and the distribution of the sources S in the ocean to get the Green's function between A and B. It is not easy to get a vertical distribution of sources in the water column. As noted in the introduction, one possibility could be to use one acoustic source dropped from a plane or a boat and that slowly sinks from the surface to the bottom while emitting repetitively an acoustic beacon during its descent. Furthermore, one could show that a drift of the source during its descent would not degrade the estimation of the Green's function as long as it remains in the AB plane. Another artificial source in the ocean

is the acoustic noise made by boats. Unfortunately, these sources are distributed horizontally along the boat path and they do not excite similarly all the modes in the waveguide. A last potential acoustic source in the ocean is noise due to surface waves, internal waves or more generally acoustic noise due to random fluctuations of the ocean. Actually, the first experimental demonstration of the Green's function estimation by secondary sources has been performed using very low thermal fluctuations in an aluminium sample [11]. The advantage of using random fluctuations as a source is the natural equidistribution of the acoustic energy over all the modes of the waveguide. Similarly, in underwater acoustics, it would be interesting to try to estimate the Green's function between points A and B simply by averaging the correlation of the noise received in A and B. Experimentally speaking, this only requires broadband receivers with a high sensitivity and a noiseless powerful amplifier. Numerical and experimental works are pursued in this direction by the first author at his new address and by another team in geophysics [15].

Finally, this work leads to application in discrete underwater acoustic communications. Indeed, beyond the quality of acoustic transmission in shallow water, an important issue is the discretion of the communication between two points in the ocean. As mentioned earlier, it has been shown that time-reversal could be a good way to transmit high-rate information through an acoustic channel without being limited by the problem of multipath propagation in such an environment. However, time-reversal is a two-step experiment and the first step requires the acquisition of the impulse response between the focal point and the TRM. This stage is not discreet because the source used at the focal point reveals the place to which information is to be transmitted in a second step. On the contrary, the technique described in this paper offers the advantage of using secondary sources to acquire the impulse response between the focal point and the TRM. This allows the focal point to remain discreet in the whole time-reversal experiment. However, acoustic transmission is usually carried out by signals in the kHz range,

which is far above the spectrum ranges studied in this work (100-300 Hz). Working at a higher frequency does not change the physical insight described in this work but, depending on the environment, it may practically require a very fine depth-step between two neighboring sources S in order to adequately sample the higher-order modes that contribute to the Green's function.

References

[1] M. Fink, "Time-reversed acoustics", *Physics Today, 50, N3, pp. 34-40, 1997.*

[2] M. Fink, "Time-reversed acoustics", *Scientific American, 281, N5, pp. 67-73,1999.*

[3] W.A. Kuperman, W.S. Hodgkiss, H.C. Song, T. Akal, C. Ferla and D.R. Jackson, "Phase conjugation in the ocean : experimental demonstration of an acoustic time-reversal mirror", *J. Acoust. Soc. Am., 103(1), pp. 25-40, 1998.*

[4] H.C. Song, W.A. Kuperman and W.S. Hodgkiss, "A time-reversal mirror with variable range focusing", *J. Acoust. Soc. Am., 103 (6), pp. 3234-3240, 1998.*

[5] P. Roux and M. Fink "Time-reversal in a waveguide : study of the spatial and temporal focusing", *J. Acoust. Soc. Am., 107 (5), pp. 2418-2429, 2000.*

[6] G.F. Edelmann, T. Akal, W.S. Hodgkiss, S. Kim, W.A. Kuperman, H.C. Song "Underwater acoustic communication using time-reversal self-equalization", *submitted to IEEE Trans. Ultrason. Ferroelect. Freq. Contr., Sept. 2000.*

[7] M. Siderius, D.R. Jackson, D. Rouseff and R. Porter, "Multipath compensation in shallow water environments using a virtual receiver", *J. Acoust. Soc. Am., 102 (6), pp. 3439-3449, 1997.*

[8] P.D. Mourad, D. Rouseff, R.P. Porter and A. Al-Kurd, "Source localization using a reference wave to correct for oceanic variability", *J. Acoust. Soc. Am., 92 (2), pp. 1031-1039, 1992.*

[9] R.P. Porter, P.D. Mourad and A. Al-Kurd, "Wave-front reconstruction in variable, multimode waveguides", *J. Opt. Soc. Am. A, 9 (11), pp. 1984-1990, 1992.*

[10] A.M. Thode, "Source ranging with minimal environmental information using a virtual receiver and waveguide invariant theory", *J. Acoust. Soc. Am., 108 (4), pp. 1582-1594, 2000.*

[11] R.L. Weaver and O.I. Lobkis, "Ultrasonics without a source : Thermal fluctuation correlations at MHz frequencies", *Phys. Rev. Letters, Vol. 87, N13, Sept. 2001.*

[12] C. Draeger and M. Fink, "One-channel time-reversal in chaotic cavities: theoretical limits", *J. Acoust. Soc. Am., 105 (2), pp. 611-617, 1999.*

[13] M.D. Collins and E.K. Westwood, "A higher-order energy-conserving parabolic equation for range-dependent ocean depth, sound speed and density", *J. Acoust. Soc. Am., 89, pp. 1068-1075, 1991.*

[14] A. Derode, A. Tourin and M. Fink, "Ultrasonic pulse compression with one-bit time reversal through multiple scattering", *Journal of Applied Physics, 85, pp. 6343, 1999.*

[15] Campillo et al….

Captions

Fig.1: Schematic of an acoustic waveguide. A and B are receivers. The secondary sources S are distributed over the whole water column: (a) the sources S are located between A and B; (b) the sources S are located outside the channel delimited by A and B.

Fig. 2: Description of the acoustic channels used for computation. The sound velocity profile c(y) linearly decreases from 1500 m/s at the surface to 1460 m/s at 25 m and then remains constant in the water column. The bottom density, sound speed and attenuation are respectively 1850 kg/m^3, 1800 m/s and 0.25 dB/λ; on the left side of the channel, 25 receivers (A_i's) span the water column; (a) range-independent case: water depth=100 m; receiver depth (B) is 40 m ; (b) range dependent case: water depth varies from 100 m on the left side to 50 m at a 2500-m range and then back from 50 m to 100 m on the right side; receiver depth (B) is 40 m. Configuration 1 or 2 refers to the positions of the secondary sources S with respect to A and B. Note that for the range-dependent case (b), configuration 2 implies more sources S than configuration 1.

Fig. 3: Spatial-temporal representation of the field received on the TRM made of the A's after transmission from B of a 0.02 s-duration pulse. The acoustic channel is described in Fig. 2a. The source depth is 40 m. Time is along the x-axis, the y-axis corresponds to depth.

Fig. 4: Spatial-temporal representation in dB of the computed time-reversed field Refoc (y, t) in the plane of receiver B after back-propagation through the channel. The TRM is made of the 25 Ai's. This time-reversed field has been computed with the exact Green's functions following Eq. 12 and is defined as the reference time-reversed field. Time is along the x-axis, the y-axis corresponds to depth.

Fig. 5: Spatial-temporal representation in dB of the computed time-reversed field $\overline{\mathrm{Refoc}}(y,t)$ in the plane of receiver B after back-propagation through the channel. The TRM is made of the 25 Ai's. The

time-reversed field has been computed with the estimated Green's functions following Eq. 13 and is to be compared to the reference time-reversed field in Fig. 4. The estimated Green's functions has been obtained from Eq. 10 (configuration 1) with a different number of sources S: (a) 50 sources S with a 2-m depth step; (b) 20 sources S with a 5-m depth step; (c) 10 sources S with a 10-m depth step; (d) 5 sources S with a 20-m depth step. Time is along the x-axis, the y-axis corresponds to depth.

Fig. 6: Comparison in dB between the envelope of the time-reversed fields $\overline{\mathrm{Refoc}}(y,t)$ and Refoc (y, t) in B (receiver depth = 40 m). The solid line corresponds to the reference time-reversed field. The estimated Green's functions have been computed with respectively 50 sources S with a 2-m depth step (dashed line), 20 sources S with a 5-m depth step (dotted line), 10 sources S with a 10-m depth step ('o' line) and 5 sources S with a 20-m depth step ('-+-' line). The sources S are placed between A and B (configuration 1).

Fig. 7: Spatial-temporal representation in dB of the computed time-reversed field $\overline{\mathrm{Refoc}}(y,t)$ in the plane of receiver B after back-propagation through the channel. The TRM is made of the 25 Ai's. The time-reversed field has been computed with the estimated Green's functions following Eq. 13 and is to be compared to the reference time-reversed field in Fig. 4. The estimated Green's functions has been obtained from Eq. 10 (configuration 1) with 25 sources S that do not span the whole water column: (a) the sources S are distributed between 1 and 49 m with a 2-m step; (b) the sources S are distributed between 50 and 99 m with a 2-m step. Time is along the x-axis, the y-axis corresponds to depth.

Fig. 8: Comparison in dB between matrices $10\log_{10}(C_{nm}(S))$ computed in different configurations of the sources S: (a) 50 sources S with a 2-m depth step; (b) 20 sources S with a 5-m depth step; (c) 10 sources S with a 10-m depth step; (d) 5 sources S with a 20-m depth step. A good estimation of the Green's function between A and B is obtained when C_{nm} is close to the Identity matrix.

Fig. 9: Standard deviation between $C_{nm}(S)$ and the Identity matrix with respect to the number of sources S. For a given number of sources S, several positions of the array of sources S may be possible in the water column leading to one or a few points for each abscissa.

Fig. 10: Range-independent case: comparison between the exact Green's function $G(A,B,t)$ in (a) and the estimated Green's function $\tilde{G}(A,B,t)$ in (b) and (c). (b) and (c) correspond to sources S located between (configuration 1) or outside (configuration 2) A and B respectively. The depth of points A and B are 37 m and 40 m respectively, (cf. Fig. 2a). The estimated Green's functions are computed from 20 sources S with a 5-m depth step.

Fig. 11: Range-independent case: standard deviation Std(S) between the estimated and the exact Green's functions on the A_i's with respect to the number of sources S in the waveguide. The dark '*' and the clear '+' correspond to sources S located between (configuration 1) or outside (configuration 2) A and B respectively. For every set of sources S, Std(S) is averaged over the 25 receivers A_i's. For a given number of sources S, several positions of the array of sources S may be possible in the water column leading to one or a few points for each abscissa.

Fig. 12: Spatial-temporal representation in dB of the computed time-reversed field Refoc (y, t) in the plane of receiver B after back-propagation through the range-dependent channel. The TRM is made of the 25 Ai's. This time-reversed field has been computed with the exact Green's functions following Eq. 12 and is defined as the reference time-reversed field. Time is along the x-axis, the y-axis corresponds to depth.

Fig.13: Spatial-temporal representation in dB of the computed time-reversed field $\overline{Refoc}(y,t)$ in the plane of receiver B after back-propagation through the range-dependent channel. The TRM is made of the 25 Ai's. The time-reversed field has been computed with the estimated Green's functions

following Eq. 13 and is to be compared to the reference time-reversed field in Fig. 12. The estimated Green's functions has been obtained from Eq. 10 (configuration 1) with a different number of sources S: (a) 30 sources S with a 2-m depth step; (b) 12 sources S with a 5-m depth step; (c) 6 sources S with a 10-m depth step; (d) 3 sources S with a 20-m depth step. Time is along the x-axis, the y-axis corresponds to depth.

Fig. 14: Range-dependent case: comparison between the exact Green's function $G(A,B,t)$ in (a) and the estimated Green's function $\tilde{G}(A,B,t)$ in (b). (b) and (c) correspond respectively to 12 sources S with a 5-m depth step located between A and B (configuration 1) or 20 sources S with a 5-m depth step outside A and B (configuration 2). The depth of points A and B are 37 m and 40 m respectively, (cf. Fig. 2b).

Fig.15: Range-dependent case: standard deviation Std(S) between the estimated and the exact Green's functions on the A_i's with respect to the number of sources S in the range-dependent channel. The dark '*' and the clear '+' correspond to sources S located between (configuration 1) or outside (configuration 2) A and B respectively. Note that configuration 2 implies more sources S than configuration 1 (cf. Fig. 2b). For every set of sources S, Std(S) is averaged over the 25 receivers A_i's. For a given number of sources S, several positions of the array of sources S may be possible in the water column leading to either one or a few points for each abscissa.

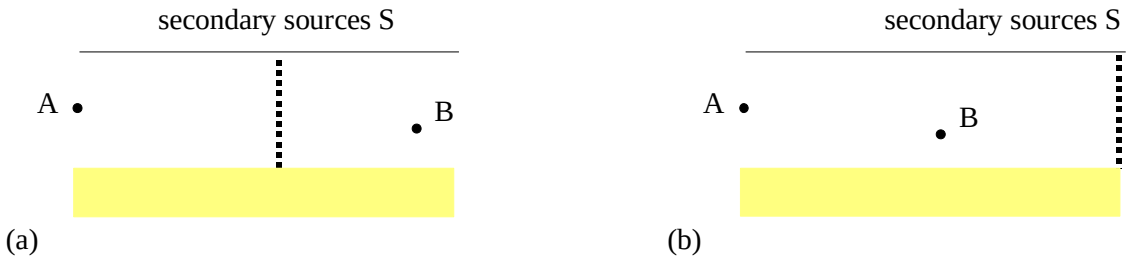

Fig.1: Schematic of an acoustic waveguide. A and B are receivers. The secondary sources S are distributed over the whole water column: (a) the sources S are located between A and B; (b) the sources S are located outside the channel delimited by A and B.

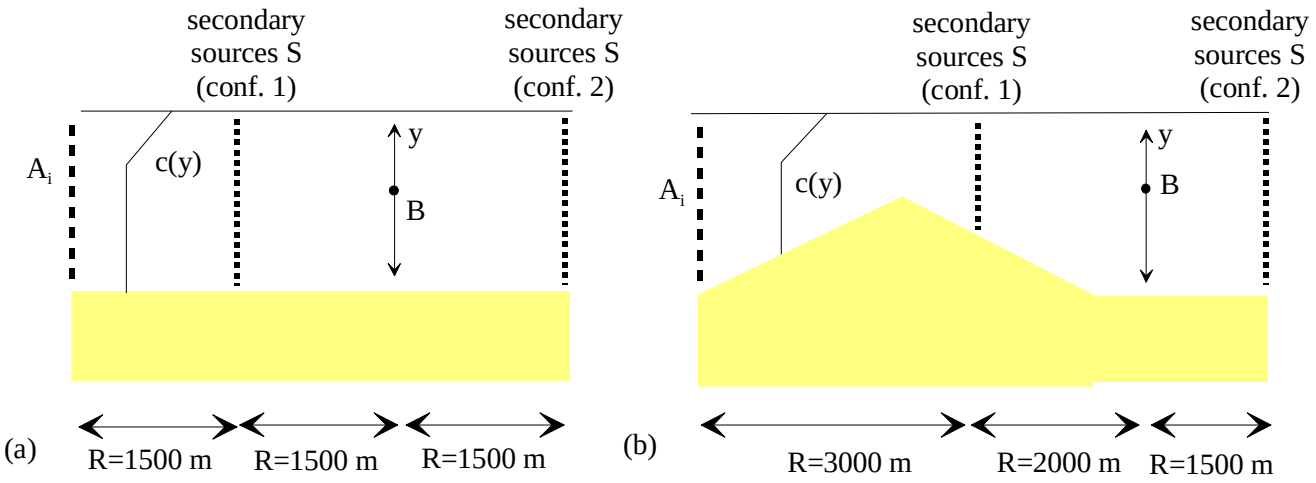

Fig. 2: Description of the acoustic channels used for computation. The sound velocity profile c(y) linearly decreases from 1500 m/s at the surface to 1460 m/s at 25 m and then remains constant in the water column. The bottom density, sound speed and attenuation are respectively 1850 kg/m^3, 1800 m/s and 0.25 dB/λ; on the left side of the channel, 25 receivers (A_i's) span the water column; (a) range-independent case: water depth=100 m; receiver depth (B) is 40 m ; (b) range dependent case: water depth varies from 100 m on the left side to 50 m at a 2500-m range and then back from 50 m to 100 m on the right side; receiver depth (B) is 40 m. Configuration 1 or 2 refers to the positions of the secondary sources S with respect to A and B. Note that for the range-dependent case (b), configuration 2 implies more sources S than configuration 1.

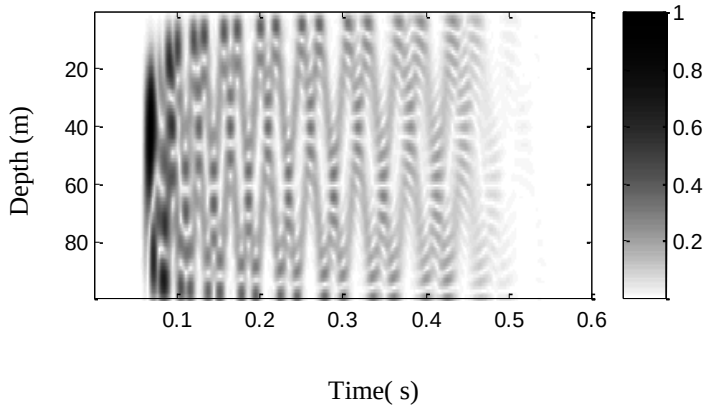

Fig. 3: Spatial-temporal representation of the field received on the TRM made of the A's after transmission from B of a 0.02 s-duration pulse. The acoustic channel is described in Fig. 2a. The source depth is 40 m. Time is along the x-axis, the y-axis corresponds to depth.

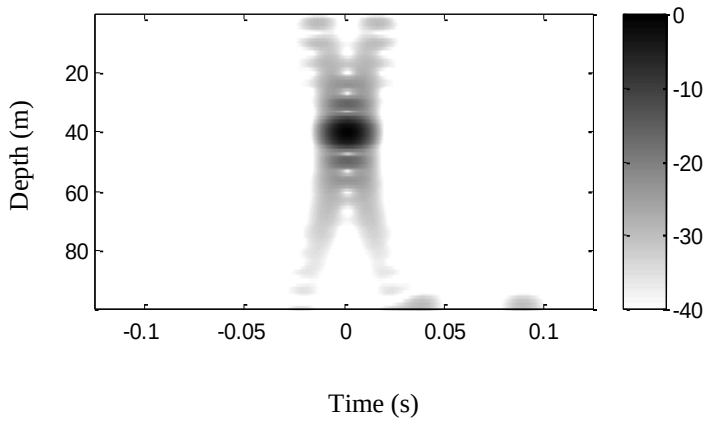

Fig. 4: Spatial-temporal representation in dB of the computed time-reversed field Refoc (y, t) in the plane of receiver B after back-propagation through the channel. The TRM is made of the 25 Ai's. This time-reversed field has been computed with the exact Green's functions following Eq. 12 and is defined as the reference time-reversed field. Time is along the x-axis, the y-axis corresponds to depth.

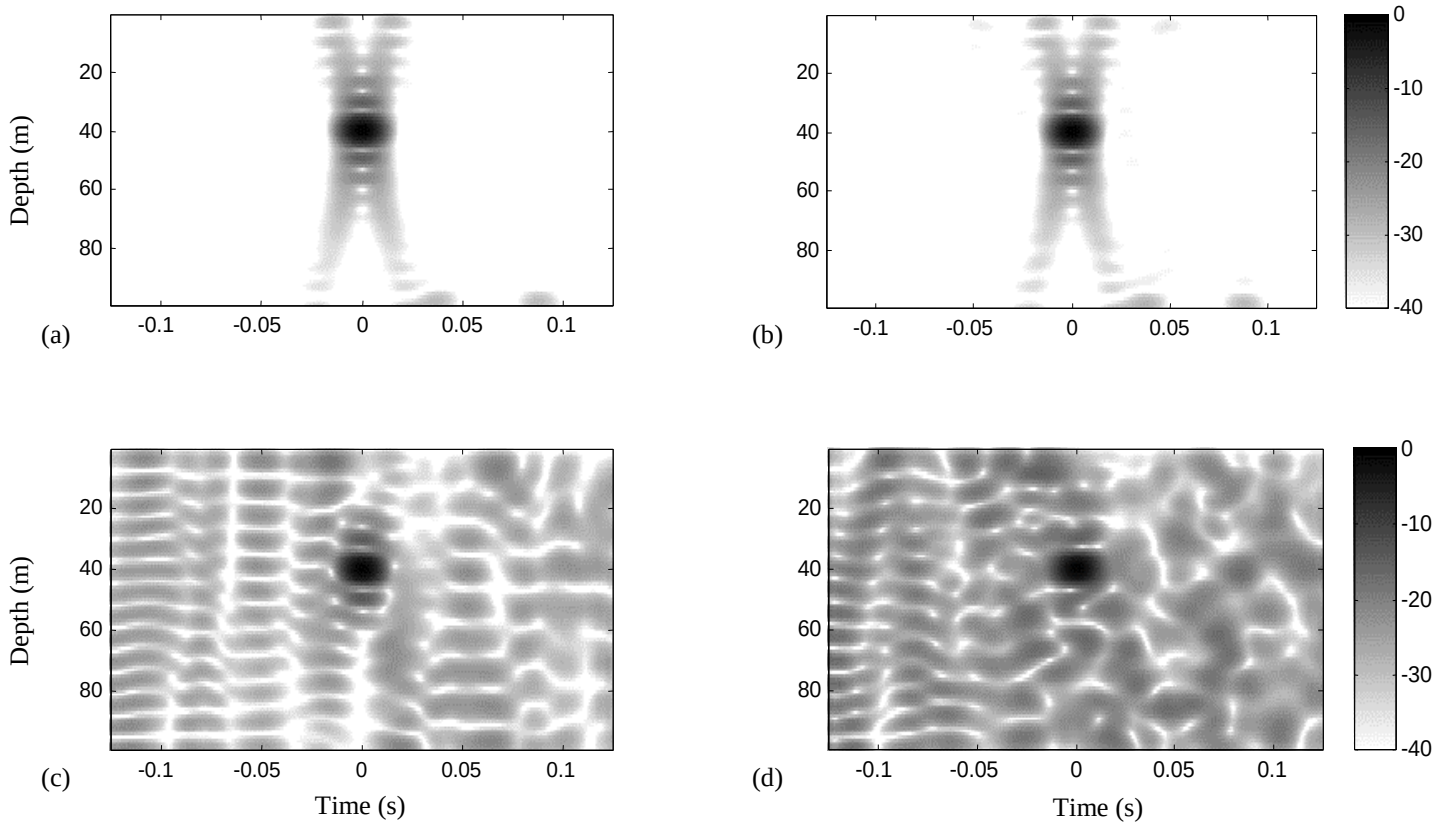

Fig. 5: Spatial-temporal representation in dB of the computed time-reversed field $\overline{\mathrm{Refoc}}(y,t)$ in the plane of receiver B after back-propagation through the channel. The TRM is made of the 25 Ai's. The time-reversed field has been computed with the estimated Green's functions following Eq. 13 and is to be compared to the reference time-reversed field in Fig. 4. The estimated Green's functions has been obtained from Eq. 10 (configuration 1) with a different number of sources S: (a) 50 sources S with a 2-m depth step; (b) 20 sources S with a 5-m depth step; (c) 10 sources S with a 10-m depth step; (d) 5 sources S with a 20-m depth step. Time is along the x-axis, the y-axis corresponds to depth.

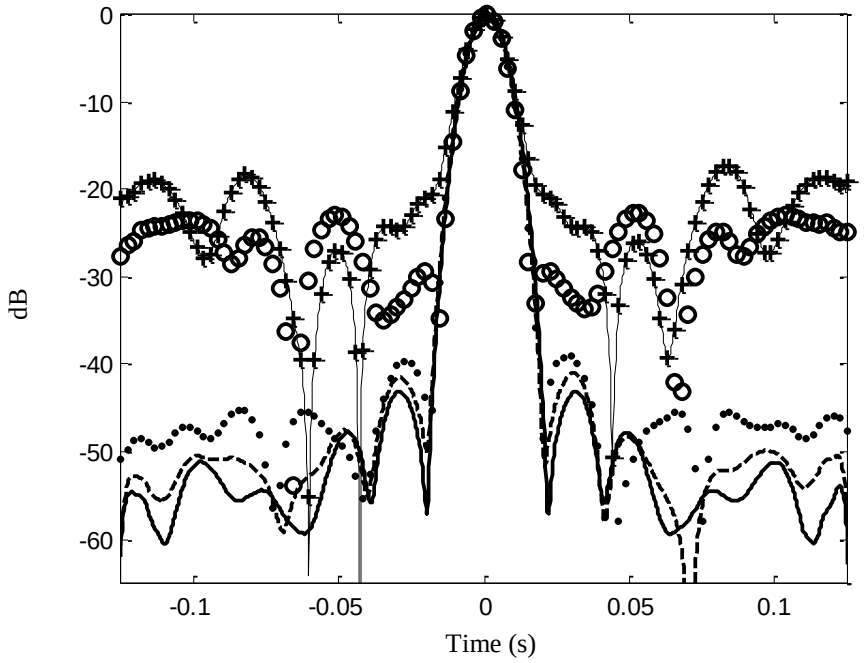

Fig. 6: Comparison in dB between the envelope of the time-reversed fields $\overline{\mathrm{Refoc}}(y,t)$ and Refoc (y, t) in B (receiver depth = 40 m). The solid line corresponds to the reference time-reversed field. The estimated Green's functions have been computed with respectively 50 sources S with a 2-m depth step (dashed line), 20 sources S with a 5-m depth step (dotted line), 10 sources S with a 10-m depth step ('o' line) and 5 sources S with a 20-m depth step ('-+-' line). The sources S are placed between A and B (configuration 1).

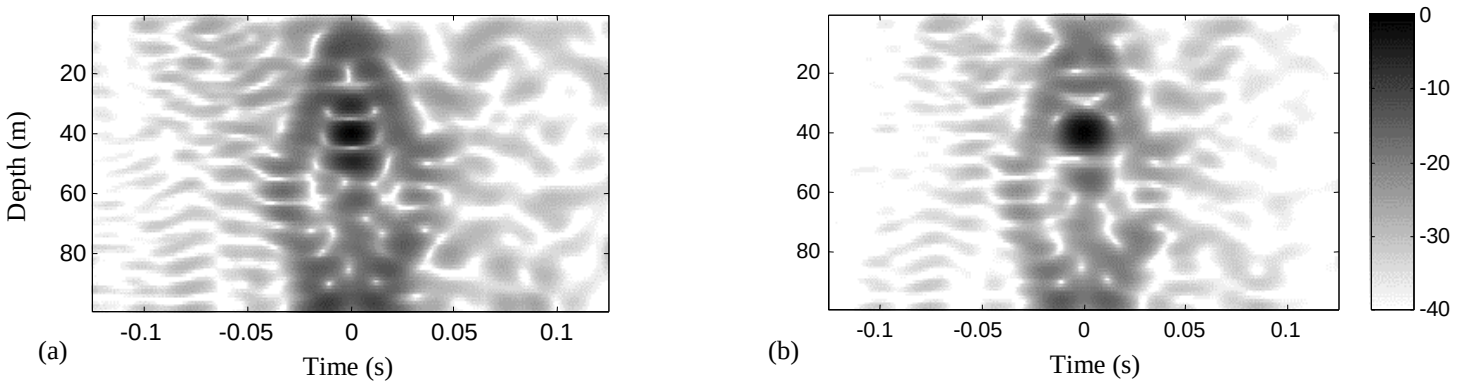

Fig. 7: Spatial-temporal representation in dB of the computed time-reversed field $\overline{\mathrm{Refoc}}(y,t)$ in the plane of receiver B after back-propagation through the channel. The TRM is made of the 25 Ai's. The time-reversed field has been computed with the estimated Green's functions following Eq. 13 and is to be compared to the reference time-reversed field in Fig. 4. The estimated Green's functions has been obtained from Eq. 10 (configuration 1) with 25 sources S that do not span the whole water column: (a) the sources S are distributed between 1 and 49 m with a 2-m step; (b) the sources S are distributed between 50 and 99 m with a 2-m step. Time is along the x-axis, the y-axis corresponds to depth.

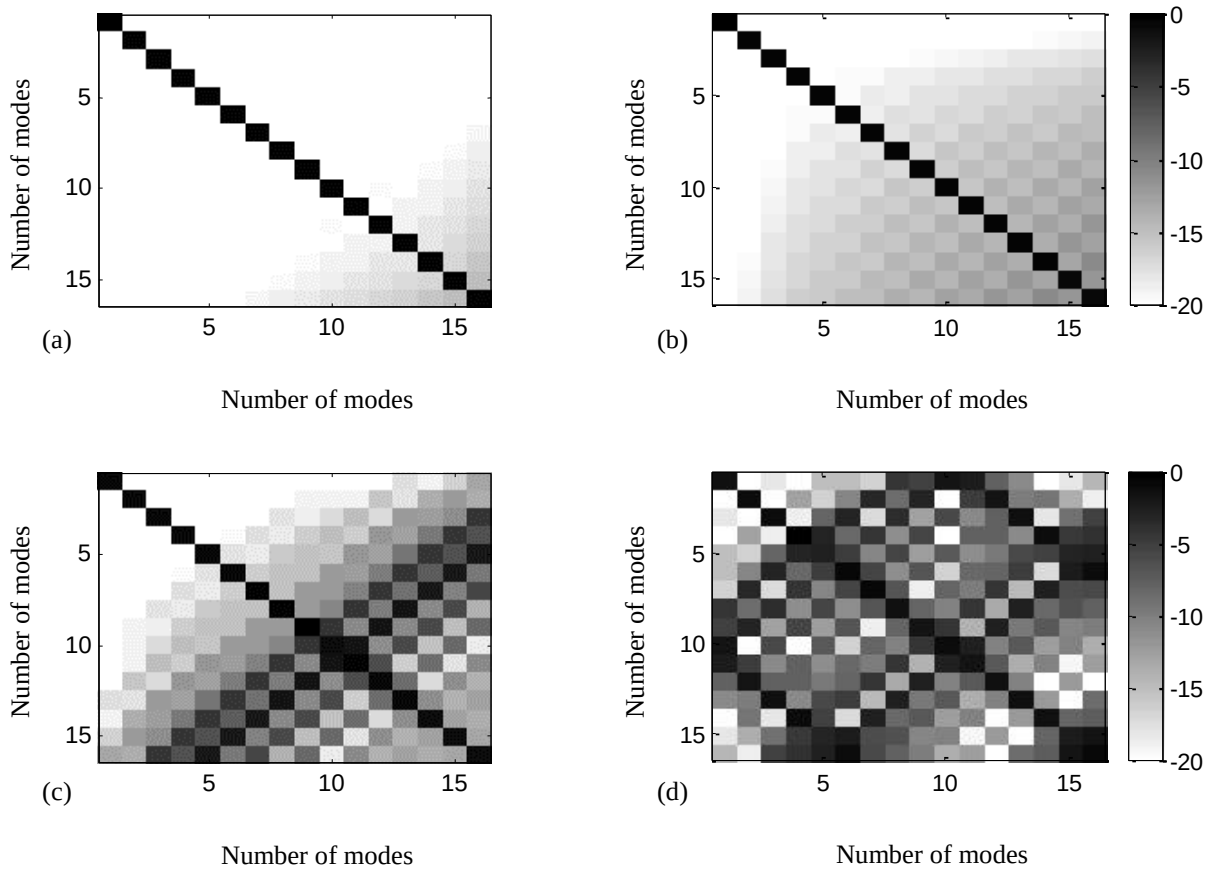

Fig. 8: Comparison in dB between matrices $10\log_{10}\left(C_{nm}(S)\right)$ computed in different configurations of the sources S: (a) 50 sources S with a 2-m depth step; (b) 20 sources S with a 5-m depth step; (c) 10 sources S with a 10-m depth step; (d) 5 sources S with a 20-m depth step. A good estimation of the Green's function between A and B is obtained when C_{nm} is close to the Identity matrix.

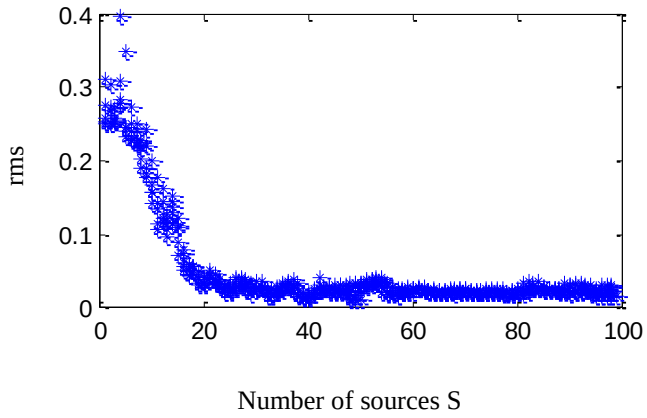

Fig. 9: Standard deviation between $C_{nm}(S)$ and the Identity matrix with respect to the number of sources S. For a given number of sources S, several positions of the array of sources S may be possible in the water column leading to one or a few points for each abscissa.

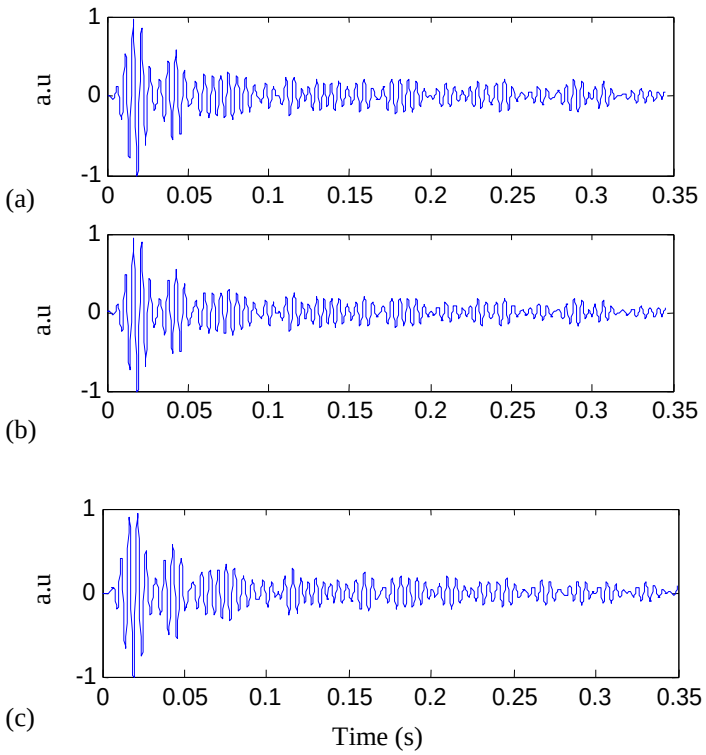

Fig. 10: Range-independent case: comparison between the exact Green's function $G(A,B,t)$ in (a) and the estimated Green's function $\tilde{G}(A,B,t)$ in (b) and (c). (b) and (c) correspond to sources S located between (configuration 1) or outside (configuration 2) A and B respectively. The depth of points A and B are 37 m and 40 m respectively, (cf. Fig. 2a). The estimated Green's functions are computed from 20 sources S with a 5-m depth step.

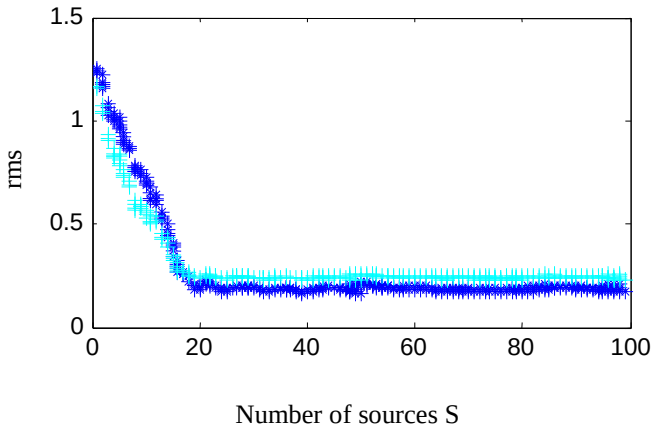

Fig. 11: Range-independent case: standard deviation Std(S) between the estimated and the exact Green's functions on the A_i's with respect to the number of sources S in the waveguide. The dark '*' and the clear '+' correspond to sources S located between (configuration 1) or outside (configuration 2) A and B respectively. For every set of sources S, Std(S) is averaged over the 25 receivers A_i's. For a given number of sources S, several positions of the array of sources S may be possible in the water column leading to one or a few points for each abscissa.

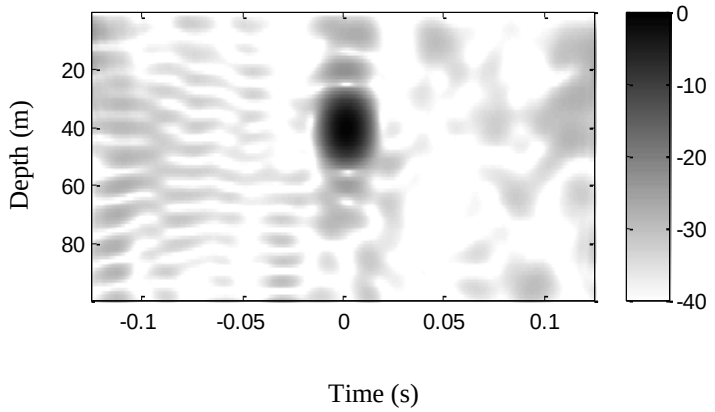

Fig. 12: Spatial-temporal representation in dB of the computed time-reversed field Refoc (y, t) in the plane of receiver B after back-propagation through the range-dependent channel. The TRM is made of the 25 Ai's. This time-reversed field has been computed with the exact Green's functions following Eq. 12 and is defined as the reference time-reversed field. Time is along the x-axis, the y-axis corresponds to depth.

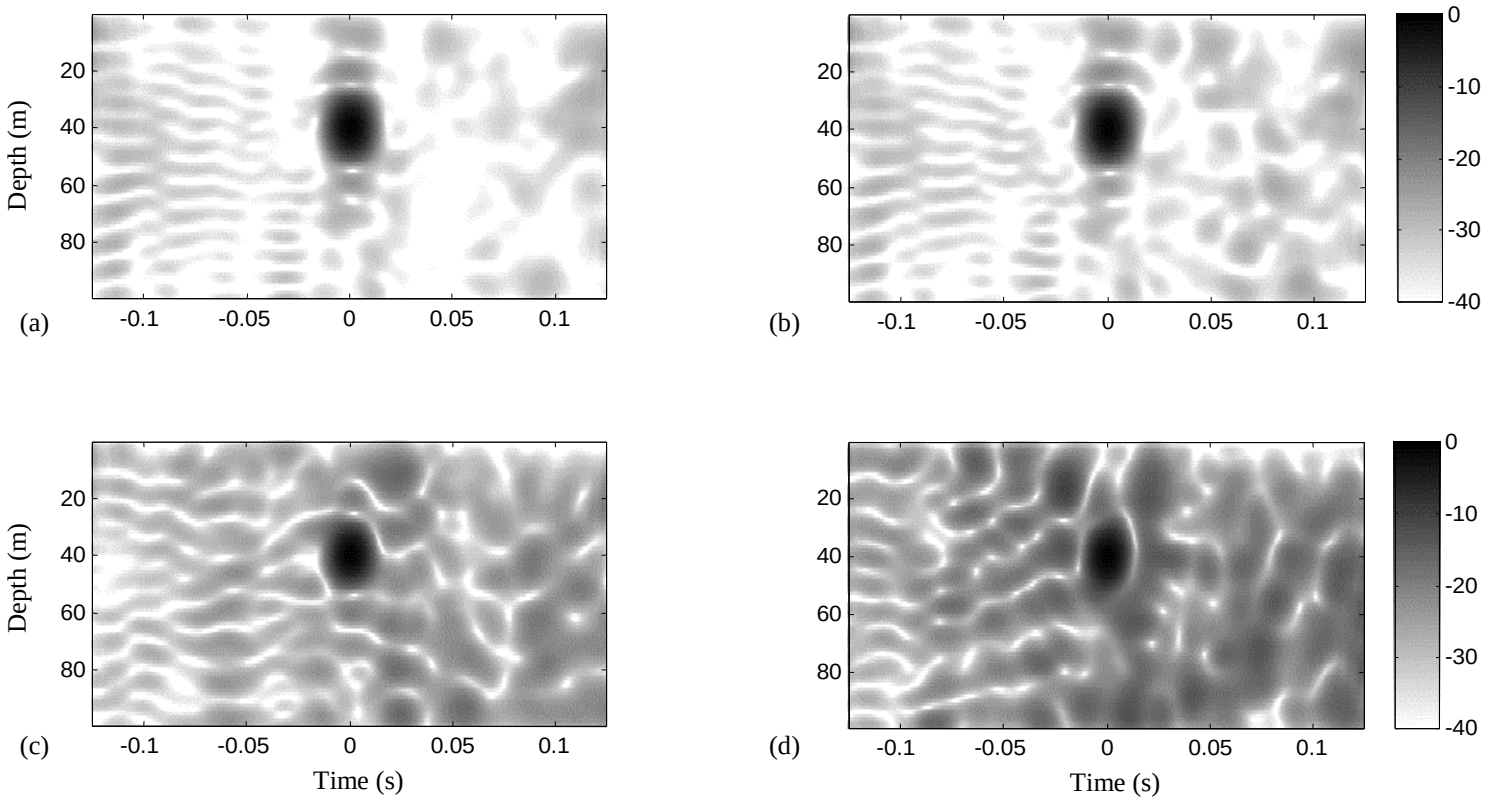

Fig.13: Spatial-temporal representation in dB of the computed time-reversed field $\overline{\mathrm{Refoc}}(y,t)$ in the plane of receiver B after back-propagation through the range-dependent channel. The TRM is made of the 25 Ai's. The time-reversed field has been computed with the estimated Green's functions following Eq. 13 and is to be compared to the reference time-reversed field in Fig. 12. The estimated Green's functions has been obtained from Eq. 10 (configuration 1) with a different number of sources S: (a) 30 sources S with a 2-m depth step; (b) 12 sources S with a 5-m depth step; (c) 6 sources S with a 10-m depth step; (d) 3 sources S with a 20-m depth step. Time is along the x-axis, the y-axis corresponds to depth.

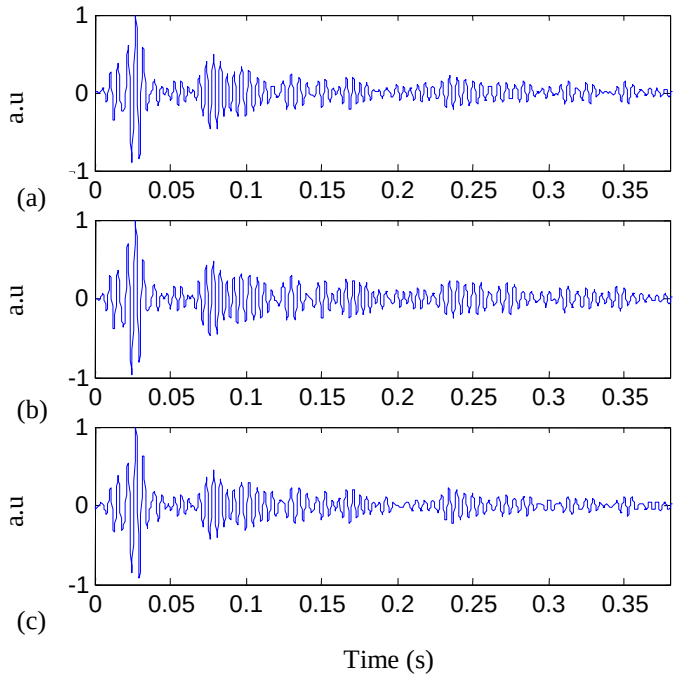

Fig. 14: Range-dependent case: comparison between the exact Green's function $G(A,B,t)$ in (a) and the estimated Green's function $\tilde{G}(A,B,t)$ in (b). (b) and (c) correspond respectively to 12 sources S with a 5-m depth step located between A and B (configuration 1) or 20 sources S with a 5-m depth step outside A and B (configuration 2). The depth of points A and B are 37 m and 40 m respectively, (cf. Fig. 2a).

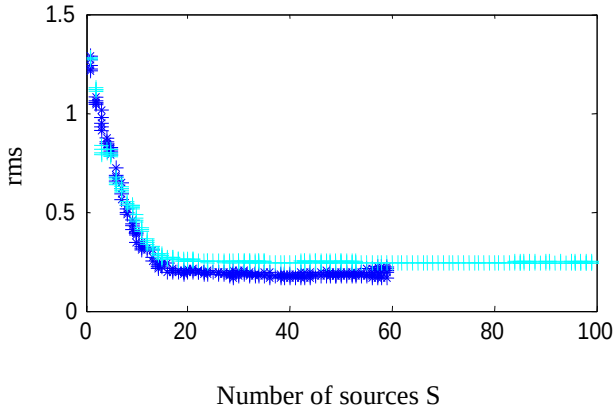

Fig. 15: Range-dependent case: standard deviation Std(S) between the estimated and the exact Green's functions on the A_i's with respect to the number of sources S in the range-dependent channel. The dark '*' and the clear '+' correspond to sources S located between (configuration 1) or outside (configuration 2) A and B respectively. Note that configuration 2 implies more sources S than configuration 1 (cf. Fig. 2b). For every set of sources S, Std(S) is averaged over the 25 receivers A_i's. For a given number of sources S, several positions of the array of sources S may be possible in the water column leading to one or a few points for each abscissa.